Timber production assessment of a plantation forest: An integrated framework with field-based inventory, multi-source remote sensing data and forest management history

Tian Gao [a,b], Jiaojun Zhu [a,b,*], Songqiu Deng [c], Xiao Zheng [a,b], Jinxin Zhang [a,b], Guiduo Shang [a,b,d], Liyan Huang [a,b,d]

[a] Key Laboratory of Forest Ecology and Management, Institute of Applied Ecology, Chinese Academy of Sciences, Shenyang 110016, China

[b] Qingyuan Forest CERN, Chinese Academy of Sciences, Shenyang 110016, China

[c] Institute of Mountain Science, Shinshu University, Nagano 399-4598, Japan

[d] University of Chinese Academy of Sciences, Beijing 100049, China

* Correspondence author at: 72 Wenhua Road, Shenyang 110016, China. Tel.: +86-24-83970342; Fax: +86-24-83970300. E-Mail: jiaojunzhu@iae.ac.cn (J.J. Zhu).

Abstract

Timber production is the purpose for managing plantation forests, and its spatial and quantitative information is critical for advising management strategies. Previous studies have focused on growing stock volume (GSV), which represents the current potential of timber production, yet few studies have investigated historical process-harvested timber. This resulted in a gap in a synthetical ecosystem service assessment of timber production. In this paper, we established a Management Process–based Timber production (MPT) framework to integrate the current GSV and the harvested timber derived from historical logging regimes, trying to synthetically assess timber production for a historical period. In the MPT framework, age-class and current GSV determine the times of historical thinning and the corresponding harvested timber, by using a “space-for-time” substitution. The total timber production can be estimated by the historical harvested timber in each thinning and the current GSV. To test this MPT framework, an empirical study on a larch plantation (LP) with area of 43,946 ha was conducted in North China for a period from 1962 to 2010. Field-based inventory data was integrated with ALOS PALSAR (Advanced Land-Observing Satellite Phased Array L-band Synthetic Aperture Radar) and Landsat-8 OLI (Operational Land Imager) data for estimating the age-class and current GSV of LP. The random forest model with PALSAR backscatter intensity channels and OLI bands as input predictive variables yielded an accuracy of 67.9% with a Kappa coefficient of 0.59 for age-class classification. The regression model using PALSAR data produced a root mean square error (RMSE) of 36.5 m^3 ha^{-1}. The total timber production of LP was estimated to be 7.27 × 10^6 m^3, with 4.87 × 10^6 m^3 in current GSV and 2.40 × 10^6 m^3 in harvested timber through historical thinning. The historical process-harvested timber accounts to 33.0% of the total timber production, which component has been neglected in the assessments for current status of plantation forests. Synthetically considering the RMSE for predictive GSV and misclassification of age-class, the error in timber production were supposed to range from -55.2 to 56.3 m^3 ha^{-1}. The MPT framework can be used to assess timber production of other tree species at a larger spatial scale, providing crucial information for a better understanding of forest ecosystem service.

Keywords: larch plantation; growing stock volume; harvested timber; age-class; radar backscatter; ALOS PALSAR; Landsat-8 OLI; random forest model; logging regime

1 Introduction

Timber production is the most important ecological services of plantation forests (Costanza et al. 1997). With development of human society, the demand of timber increases sharply. Timber production of natural forest hardly meet timber demand of human society due to deforestion of primary forest across the world, thus plantation forests are planted as a substitution for natural forests (Mason and Zhu 2014; Zou et al. 2015). As reported by Food and Agriculture Organization (FAO) in 2010, the total area of planted forest is estimated to be 264 million ha, corresponding to 6.6% of the world's forest area. During the past half century, China possesses the largest area of planted forests in the world, accounting for 36% (69 million ha) of the country's total forested area. whereas only accounting for 17% (2.48×10^9 m^3) of the total growing stock volume (GSV), with an average of 35.8 m^3 ha^{-1} (Chinese Ministry of Forestry 2014). The low productivity weakens the expected function of plantation forests for timber production. In this context, accurate estimation of timber production and its spatial distribution are required for a better understanding of ecological service functions and further improving timber production of plantation forests, which services for the strategic goals of plantation forest resource management (Alkemade et al. 2014; Mason and Zhu 2014; Fu and Forsius 2015).

The GSV is defined as stem volume of living trees in a given area of forest, including bark but excluding branches and stumps. The GSV represents directly the amount of current timber in a stand, which is a key indicator in the context of forest management. GSV is also a major predictor for assessing biomass of forest, which plays an important role in carbon cycle and global change issues (Fang et al. 2001; Pan et al. 2011). The GSV is traditionally estimated from field-based measurements of the diameter at breast height (DBH) collected at sample plots (Santoro et al. 2011). Alternatively, the satellite-based approach aided by forest inventory can up-scale observed extent and has thus been widely used to estimate GSV or biomass for a continuous spatial distribution (Bijalwan et al. 2010; Gao et al. 2013a). Satellite optical images have been used to estimate biomass and GSV at different scales (Houghton et al. 2007; Anaya et al. 2009; Zheng et al. 2013; Gao et al. 2013b). However, passive optical data can only sense the canopy in two dimensions, thereby making it be insensitive to sub-canopy structure, such as basal area and height of tree (Almeida Filho et al. 2007; Morel et al. 2011). Satellite-based synthetic aperture radar (SAR) data have been examined for handling this issue, due to their sensitivity to the geometric properties of forests (Liesenberg and Gloaguen 2013; Chowdhury et al. 2014; Galeana-Pizaña et al. 2014; Santoro et al. 2015). Comparing to SAR data acquired at shorter wavelengths (e.g., X and C-bands), L-band (23.5 cm) SAR is particularly useful in mapping forest areas because of its better ability to penetrate into forest canopies. The L-band backscatter from forested terrain consists primarily of backscatter from stem volume (Way et al. 1994; Karam et al. 1995), thus showing greater sensitivity to the woody components. In current studies, L-band SAR data have also been proved to be more useful for GSV estimation (Imhoff 1995; Simard et al. 2002; Rosenqvist et al. 2007), although a saturation effect (L-band backscatter does not increase with GSV) has been observed. Previous literatures reports that L-band

SAR data appears well adapted to estimate the relatively low GSV of boreal forest (Peregon and Yamagata 2013; Suzuki et al. 2013), temperate forest (He et al. 2011; Cartus et al. 2012) and savanna woodlands (Carreiras et al. 2012; Mermoz et al. 2014). However, these studies on L-band SAR data-based GSV estimations are specific to each study site that caused by various environment conditions and forest structures. Considering that low GSV and structure of plantation forests in China, L-band SAR data are supposed be rather useful for the GSV estimation of plantation forests, but little attention has been paid to the issue.

Timber production of plantation forests is a historical process, closely relating to forest managements. In addition to current GSV, thinning operation (or selective logging), which is considered as a component of near-natural forest management (Luo et al. 2014; Li et al. 2014a), also harvests considerable biomass, including non-timber and timber biomass. For an efficient forest management, successive thinning should be implemented as a stand growing, providing timber throughout a rotation of plantation forest. During this stand age-related process, additionally, non-timber biomass of plantation, including branches and leaves, is returned to soil or collected for fuelwood. These forest management practices have been recognized to play an important role in the terrestrial carbon cycle and the potential contribution to climate change mitigation efforts for plantation forests (Ray et al. 2009). Nevertheless, due to the extensive area of plantation forests and the long-term history of forest management, our current knowledge about the timber production of historical process is rather limited. Previous studies have reported the effects of thinning on carbon storage

(Davis et al. 2009; Nunery and Keeton 2010) and structure (Forshed et al. 2008; Zhu et al. 2010) at a stand-scale, however, these studies mainly focused on the responses of forest to management practices. Yet few studies have investigated the historical contribution of successive thinning operations to timber production at a continuous spatial scale. Although a long-term field-based inventory that recording management practices can represent the historical timber production for a given stand, it is insufficient for a large spatial scale assessment of production timber. This resulted in a gap in a synthetical ecosystem service assessment of timber production of plantation forests.

In order to obtain timber production for a period, the timber harvested by historical management practices is supposed to be quantitated. In this study, timber is defined as stem volume of trees, and timber production includes harvested timber and current timber (GSV). We established a Management Process–based Timber production (MPT) framework to integrate historical logging process and current potential of timber production, trying to synthetically assess timber production for a historical period at a continuous spatial scale. In the MPT framework, age and current GSV of plantation forests are the two key parameters, and a space-for-time substitution was used to defining historical process-harvested timber. To test and apply this framework, we conducted an empirical study on a larch plantation (LP) in Saihanba Forestry Center, which is the largest plantation forest center of larch in Asia. Multi-source remote sensing data and field-based inventory were employed to estimate age and GSV of plantation forests. These two key parameters are input to the MPT framework to assess the timber production for a period of approximate 50 years.

2 Data and Methods

2.1 Study area

Larix spp. is one of the most important planted timber tree species of China (Zhu et al. 2010; Yan et al. 2013; Gao et al. 2015). Since the 1950s, about 3.06 million ha of LP have been planted in North China. This study location is Saihanba Forestry Center (SFC), which is the largest plantation forest center of larch in Asia (116°52–117°39′ E, 42°04′–42°36′ N; *ca.* 93,000 ha; Fig. 1). SFC is located in a typical forest-steppe ecotone between the Inner Mongolian Plateau and North Hebei Mountain, with an elevation ranging from 1042 m to 1936 m. The climate of SFC is semi-arid and semi-humid, with a short growing season of May to September. Annual mean air temperature and precipitation were -1.2 °C and 452 mm, respectively. SFC consisted of six sub-forestry centers, by the names of Sandaohekou (SDHK), Qiancengban (QCB), Beimandian (BMD), Yinhe (YH), Sanxiang (SX), Dahuanqi (DHQ), from west to east, respectively. Since 1960s, SFC has planted over 74,000 ha of plantation forest. Currently, the forest cover of SFC reaches as high as 80%. The total extent of LP (*Larix principis-rupprechtii*, a principal tree species for forestation) is approximately 44,000 ha, accounting for 58% of forest land area of SFC. Most of LPs in SFC are a single species monoculture. The other forest types are *Pinus sylvestris var. mongolica* plantations and *Betula platyphylla* natural secondary forest, accounting for 27% and 11% of total forest area, respectively.

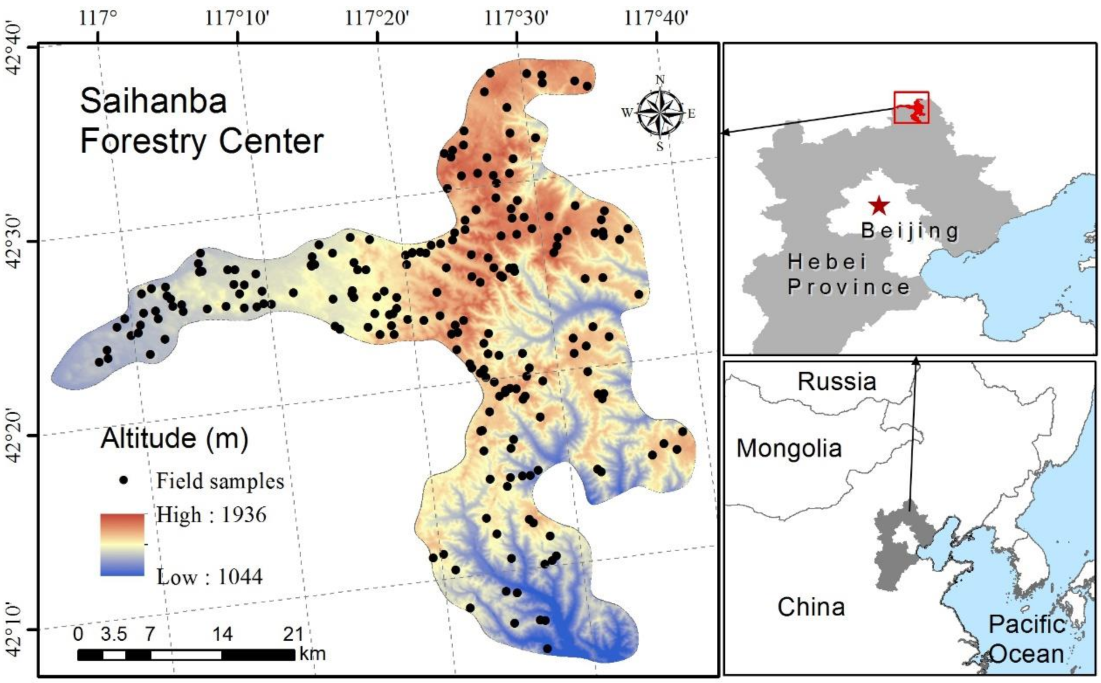

Fig. 1. Location of Saihanba Forestry Center and spatial distribution of sampling sites.

2.2 Logging regime of SFC

The logging operations in the study area are regulated by the forest management of SFC. Generally, LP rotation is approximately 40 years. During this period, LP experiences 5 thinning operations. For each thinning operation, approximate 20% of GSV is harvested for a stand. The first thinning operation is carried out when LP is 16 to 19 years. Then, thinning operation is carried out every 4 or 5 years. The last thinning operation was conducted when LP is 37 to 39 years old. Finally, LP is clear-cut after they are older than 40 years. A small portion of LPs that are older than 45 years may be reserved to produce large-diameter timber.

2.3 Field data

Two field surveys were conducted and 77 plots of LP were sampled during summer (July and August) of 2013 and 2014. Each plot had a dimension of 30 × 30 m, where was settled at least 15 m far from boundary of a LP patch to ensure its representative. On each plot, DBH was measured for every tree with its diameter ≥ 4 cm. Stand density and age were recorded. Thinning operation roughly in last five years was also recorded by counting stumps in a sampling plot. Since the larch is originally planted as patches, the forest structure within a patch is relatively homogeneous. Therefore, the plot-level investigation could generally represent the situation of a LP stand. In addition to the above sample data, we also collected Forest Resource Management Inventory (FRMI) data derived from SFC in 2011. FRMI is usually conducted by local forestry administrations, aiming to support forest management and production (Zeng and Zhou 2003). In this study, the field information extracted from these data to supplement our field surveys. A total of 215 samples were finally obtained. These larches grown across a forest-steppe ecotone that is unique in climatic conditions and soil backgrounds, under which these trees likely had a unique architecture such as crown shape, woody element arrangement, and stem taper that determines the stem volume equation. This determination can not be more accurately reflected by a regional or national stem volume equation (Jenkins et al 2003); therefore, a local stem volume equation (Saihanba Forestry Center, 2012) was used to estimate the stem volume of the sampled trees. The equation is given by:

$$V = 0.00009521 \times D^{2.56180452} \tag{1}$$

where V is stem volume (m^3) and D is DBH (m). The total GSV of each plot is calculated as the sum of all trees in a plot. The calculated results for 215 samples represented GSV of LP for the period of 2011, 2013 and 2014. To correspond temporally to remote sensing data (2010), an empirical annual increment of GSV and the records of thinning were employed to adjust the GSV value to that of 2010.

2.4 Remote sensing data and pre-processing

2.4.1 ALOS PALSAR

The ALOS PALSAR (Advanced Land-Observing Satellite Phased Array L-band Synthetic Aperture Radar) data used in this study consisted of 1 × 1 degree (*ca.* 111 × 111 km) mosaic tiles at a spatial resolution of 25 × 25 m for 2010, which was provided by JAXA (Japan Aerospace Exploration Agency). The strip data that show minimum response to surface moisture were preferentially selected for the period of 2010 (Shimada et al. 2014). The dataset has been geometrically corrected using the 90 m SRTM Digital Elevation Model, as well as radiometrically calibrated and balanced for seasonal change between adjacent strips (Shimada and Ohtaki 2010). Two tiles were combined to generate a mosaic for study area at HH (horizontal transmit and horizontal receive) and HV (horizontal transmit and vertical receive) polarizations. A median filter with a window size of 5 × 5 pixel was applied to reduce speckle effects (Lee et al. 2009; Shimada et al. 2014). Because spatial resolution of Landsat-8 OLI (Operational Land Imager) is 30 × 30 m, the PALSAR images were resampled to the resolution of 30 × 30 m for the consistency of remote sensing dataset. The PALSAR dataset was expressed in the form of the normalized radar cross section with gamma-naught (γ^0). The digital numbers (DN) signal was converted into backscatter coefficient γ^0 using the following equation (Shimada et al. 2009):

$$\gamma^0 = 10 \times \log 10(DN^2) - 83 \tag{2}$$

where DN stands for 16-bit unsigned integer digital numbers. The calculations of ALOS PALSAR mosaic data produced two features: HH and HV backscatter of 2010. These two PALSAR variables were used for GSV estimation.

2.4.2 Landsat-8 OLI

Landsat-8 OLI is a new sensor of the Landsat series, which has improved sensor signal-to-noise performance and associated improvements in radiometric resolution, *etc*. (Roy et al. 2014). The OLI bands consists of blue (0.45–0.51 μm), green (0.53–0.59 μm), red (0.64–0.67 μm), near infrared (0.85–0.88 μm) and two shortwave infrared (1.57–1.65 μm and 2.11–2.29 μm) bands. OLI scenes (P123/R31) in four seasons, including spring (green-up stage, 15 May 2014), summer (growing peak stage, 29 July 2013), autumn (defoliating stage, 4 October 2013), and winter (leafless and snowless stage, 4 November, 2013), were adopted. Geometric correction was performed by approximate 50 ground control points to reduce the error to less than 15m; radiometric calibration, atmospheric correction were performed using the Fast Line-of Sight Atmospheric Analysis of Spectral Hypercubes (FLAASH) software package in ENVI 5.0. Furthermore, the 4-scene OLI images were processed with the Kauth–Thomas linear transformation, which generated 12 features (brightness, greenness and wetness for 4-scene). Combining with the original bands, a total of 36 variables derived from OLI images were employed for discrimination of LP age-classes.

2.5 Random forest

Random forest (RF) was used to predict age-class of LP. Random forest is a simple but robust machine learning algorithm, which can be viewed as an ensemble of individual tree-like classifiers (Breiman 2001; Rodriguez-Galiano and Chica-Olmo 2012). It can handle a number of input variables, as well as quantify the contribution of each input variable (Rodriguez-Galiano et al. 2012). Two user parameters are required to run a RF model: the number of tree in forest (*ntree*) and the number of prediction variables used at each split to grow a decision tree (*mtry*). Breiman (2001) suggested that adding more trees to RF model does not induce over-training. More trees can strength stability of “out of bag” (OOB) error assessment. In order to obtain more reliable estimate of OOB error, we followed recommendations by Diaz-Uriarte and Alvarez De Andres (2006) and set *ntree* to 1000. Additionally, the squared root of the total number of input variables was implemented to determine *mtry* (Naidoo et al. 2012), and this assignment of *mtry* value could generate acceptable results (Liaw and Wiener 2002; Ismail et al. 2010; Naidoo et al. 2012).

2.6 Modelling timber production

2.6.1 Framework for modelling timber production

In a plantation forest ecosystem, current GSV represents standing stock of timber. In other words, it can be defined as the potential of timber production when all the trees are clear-cut. Timber producing is a successive and historical process, which closely links to forest management. Therefore, a MPT framework was elaborated which concerns current GSV and the harvested timber derived from historical logging regimes. In the framework, age was used to descript the processed management practices (historical thinning) of plantation forest; current GSV represented the current potential of timber production. As descripted in section 2.2, LP of SFC is supposed to experience 5 thinning operations during a rotation. Considering the historical logging regime of LP, a special MPT framework was designed for modelling timber production (Fig. 2).

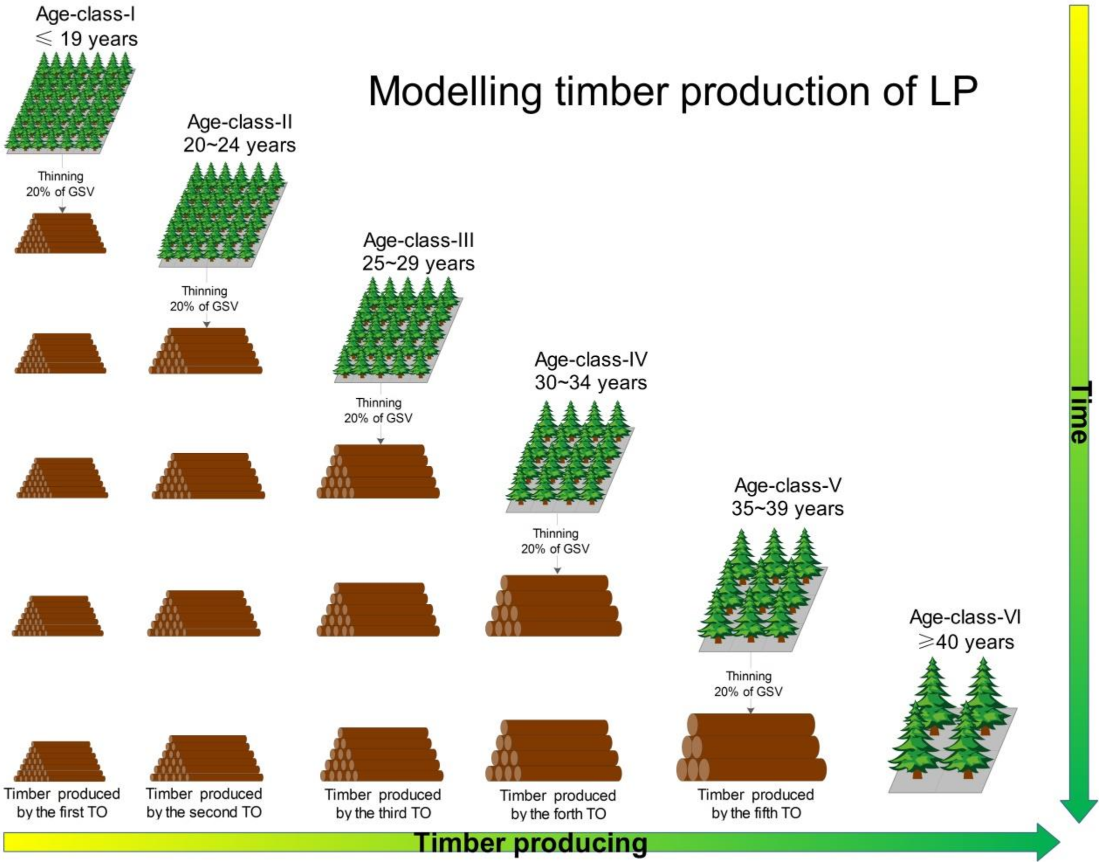

Fig. 2. A management process–based timber production framework for larch plantation of SFC. TO refers to thinning operation. Age-class-I: ≤19 years; Age-class-II: 20~24 years; Age-class-III: 25~29 years; Age-class-IV: 30~34

years; Age-class-V: 35~39 years; Age-class-VI: ≥40 years.

As descripted in Fig. 2, LP ages were divided into 6 age-classes, closely linking to the logging regime of SFC. Four age-classes were defined with an interval of 5 years between 20 and 40 years, and the other two age-classes were defined by less than 19 years and larger than 40 years, respectively. The timber production of an Age-class-I LP stand is supposed to be its current GSV. The timber production of an Age-class-II LP stand is supposed to consist of the current GSV and the harvested timber (20% of GSV) when this stand is in Age-class-I. Similarly, the timber productions of LP stand of Age-class-III, IV, V and VI were assessed, via this method (Fig. 2). For example, an Age-class-VI LP stand experiences 5 thinning operations, therefore its timber production is considered as a summation of the current GSV and harvested timber through 5 thinning operations. In the MPT framework, current GSV and historical harvested timber were summed as the total timber production of a LP stand. Historical harvested timber can be calculated by times of processed thinning operations and corresponding harvested timber for each thinning operation. Therefore, current GSV and age-class are the two key parameters of the MPT framework. The latter identifies the times of processed thinning operation of a LP stand and which thinning operations have been carried out (Fig. 2). To implement this framework, a set of predictive variables derived from PALSAR data and OLI images was created for the estimations of GSV and age-class.

The estimation of historical harvested timber derived from a specific thinning operation is a practical problem. Since the historical GSV of a LP stand cannot be obtained, a “space-for-time” substitution was employed to infer past harvested timber. In this process, current GSVs of different age-classes were adopted as the substitutions for historical GSV. For example, in order to estimate the timber productions of a LP stand of Age-class-VI, the timber harvested by the fifth thinning operation, which was carried out between 35 and 39 year (Age-class-V), is required (Fig. 2). The current GSV of Age-class-V LP stand and thinning intensity (20% of GSV) were employed to produce the required value. In order to obtain the reliable substitutions for historical harvested timber, various situations were considered. Generally, forest managements and site conditions both influence plantation forest productivity. The LP management of SFC are consistently regulated, with the similar original planting density (ca. 5000 trees ha^{-1}) and practices (thinning and pruning, etc.), thus these impacts on the historical harvested timber are limited. Site condition is another important influential factor. In SFC, larch tends to be planted in a flat area, with an altitude range of 1597 ± 168 m (statistics for 215 samples). The low variations in altitude lead a weak impact on timber production. It should be noted that aspect is a key factor, closely relating to soil properties and available water (Yimer et al. 2006). Synthetically considering these topographical factors, we divided slope range into four segments with an interval of 5°, and divided aspect into sunny slope (SW, S, and SE aspects) and shady slope (NE, N, and NW aspects). This grading generated 8 topographical types (Fig. 3).

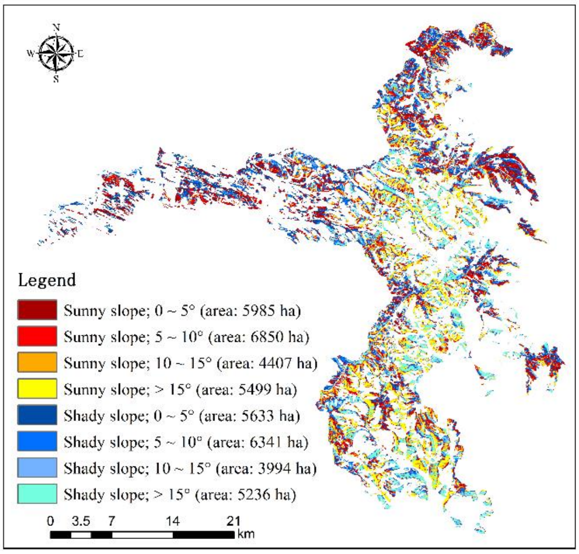

Fig. 3 The eight topographical types of SFC LP

Combined with 6 age-classes, 48 combinations were produced. By overlaid the estimated GSV, a total of 48 substitutions that calculated by averaged GSV of corresponding area, were generated for calculation of historical harvested timber. At pixel level, harvested timber and GSV were summed as timber production of LP (Fig. 4). Due to the wide range of Age-class-I (0 to 19 year), the GSV of low age (less than 15 year) LP cannot represent harvested timber of Age-class-I. Here we assume that the ages of LP are distributed evenly in the Age-class-I, and only adopt the 20% of pixels with the highest GSV to estimate the harvested timber.

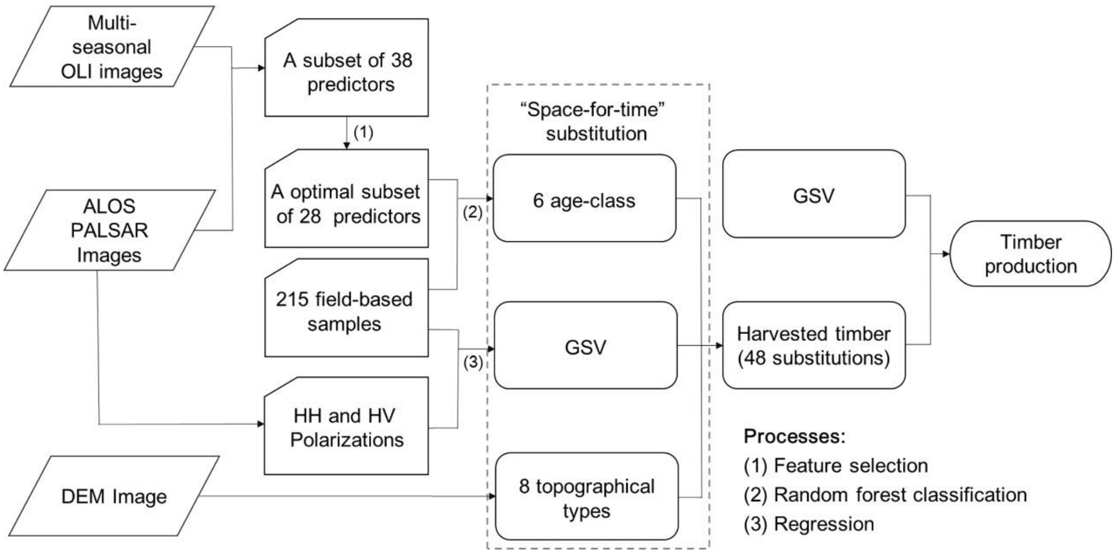

Fig. 4 Flowchart describing the process of modelling timber production of LP

2.6.2 Estimation of GSV

The calculated field-based GSV were correlated to the spatial corresponding pixel backscatter of PALSAR data (Fig. 4). The 2/3 of the total samples was used to adopt regression models with γ^{0}_{HV} and γ^{0}_{HH}, respectively. Based on the reserved samples (1/3 of the total samples), root mean squared error (RMSE) were calculated to evaluate the precision of the models.

$$\mathrm{RMSE} = \sqrt{\frac{1}{\mathrm{N}}\sum_{i=1}^{\mathrm{N}}\left(Y_{Predi} - Y_{Obsi}\right)^{2}} \tag{3}$$

Where Y_{Predi} is the ith prediction and Y_{Obsi} is the ith observation. Finally, the best regression model and band were selected and used to map GSV for the whole study area.

2.6.3 Estimation of age-class

A useful approach to estimate stand age has been to use spectral reflectance, due to its changes in chlorophyll content and the internal structure as trees gets older (Jensen et al. 1999; Dye et al. 2012). During the whole growing cycle of trees (e.g. leaf on and leaf off), remotely sensed spectral signals of different forest ages also varied (Li et al. 2014b). To capture these subtle differences in spectral response to phenological variabilities among various LP age-classes, the original six bands as well as three features produced by Kauth–Thomas linear transformation for four-season were aided for creating a set of 36 optical remotely sensed variables. Furthermore, as a plantation forest growing, its undercanopy structure changes substantially. SAR data (Section 2.4.1) can help to characterize the structure differences among varied age-class. Finally, a total of 38 variables were adapted to train RF model. In turn, the four-seasonal images and Kauth–Thomas linear transformations on the bands produced a number of variables, and some of them are probably correlated or redundant, leading to an obstacle of expected increase in accuracy (Rodriguez-Galiano et al. 2012). In order to identify the most informative predictors for the discrimination of age-class, a feature selection strategy was employed based on the RF-derived importance assessment. The optimized subsets of variables were gradually generated and further applied to a RF model to mapping LP age-classes.

A confusion matrix of prediction based on OOB error was used to assess the age-class classification accuracy. In this process, each sample in OOB (ca. 1/3 of original samples) is predicted by its corresponding bootstrap (ca. 2/3 of original samples) training tree (Grimm et al. 2008). Then, predicted categories are compared to observed categories for each individual tree to calculate OOB error. Finally, the

OOB errors for all trees in the forest are aggregated to estimate overall error. OOB error is considered to be a reliable assessment of predictive accuracy (Breiman 2001; Ismail and Mutanga 2010; Adam et al. 2014; Tinkham et al. 2014). Since OOB error does not need an independent validating dataset (Lawrence et al. 2006; Grimm et al. 2008), it is of particular interest regarding the forest area, where collection of abundant field-based samples is difficult. All RF computations of this study were performed by statistical software R 2.15.2.

3 Results

3.1 Age-class of LP

The 38 input variables were used in RF model to classify age-classes of LP. The accuracy of the RF classifier for the six age-classes was 65.6%, with a Kappa coefficient of 0.56. In order to enhance the efficiency of RF classifier, RF model identified the importance of each input variable and further produced optimal subset of possible predictors by reducing redundant predictors (Fig. 5). As reducing the weaker predictors, the classification accuracy stalled or marginally increased until a turning point that 10 variables was eliminated (slope = 0.0017; R^2 = 0.826; P = 0.013), and decreased afterwards (slope = –0.4203; R^2 = 0.772; P < 0.001). Although the neighboring points could be used to divide the fitted curve and the similar trends could be observed, the R^2 was lower than that of the 10-variable reduction. Finally, the classification of age-class was improved with the “best” subset (28 input variables), which has an overall accuracy of 67.9% and kappa coefficient of 0.59.

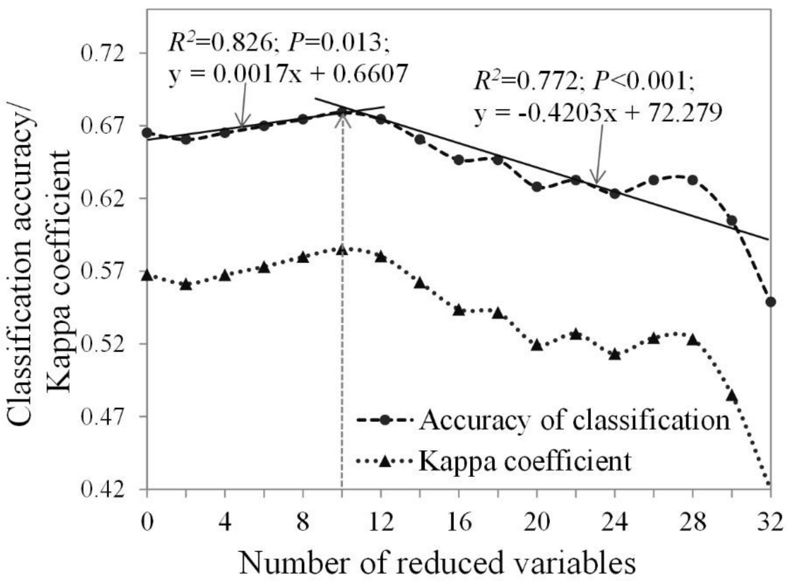

Fig. 5. The effect of variable reduction on classification accuracies.

The high producer's accuracy was observed for Age-class-I, followed by Age-class-V and Class-VI (Table 1). The lowest produce's accuracy was Age-class-III. The confusion matrix shows that there were discrepancies between the producer's and user's accuracy. For Age-class-I and V, the producer's accuracies were higher than user's accuracies; for Age-class-II and III, conversely, the producer's accuracies were lower than user's accuracies. The differences between producer's and user's accuracies of Age-class-IV and VI were rather small. This result suggested that the age-class map produced by RF model tended to misclassify other age-classes as Age-class-I and V.

Table 1 Confusion matrix of the RF classifier for the six age-classes of LP. I~VI refer to the six age-classes of LP. Prod. acc. and user acc. refer to producer's accuracy and user's accuracy, respectively.

Reference	Classify as

Data	I	II	III	IV	V	VI	total	Prod. acc.
I	49	0	0	2	1	0	52	0.942
II	2	6	0	2	4	2	16	0.313
III	5	0	3	3	8	1	20	0.150
IV	2	4	0	17	7	2	32	0.500
V	3	0	2	6	53	2	66	0.791
VI	0	0	0	2	9	18	29	0.613
total	61	10	5	32	82	25	215	-
User acc.	0.803	0.600	0.600	0.531	0.646	0.720	-	0.679

This classifier was applied to map the age-classes of LP, which was shown in Fig. 6a. The mapping result suggests that high age-classes (≥ 30 years) mainly appeared in the western part and northern part of SFC, while low age-classes (< 30 years) distributed in the eastern and southern part of SFC. This result was generally consistent with the history of SFC afforestation. Because the topography in the western and northern part of SFC is relatively flat, the initial afforestation was carried out in these areas (SDHK, QCB and BMD sub-forestry centers). Furthermore, high age-classes were also observed nearby the main roads (Fig. 6a).

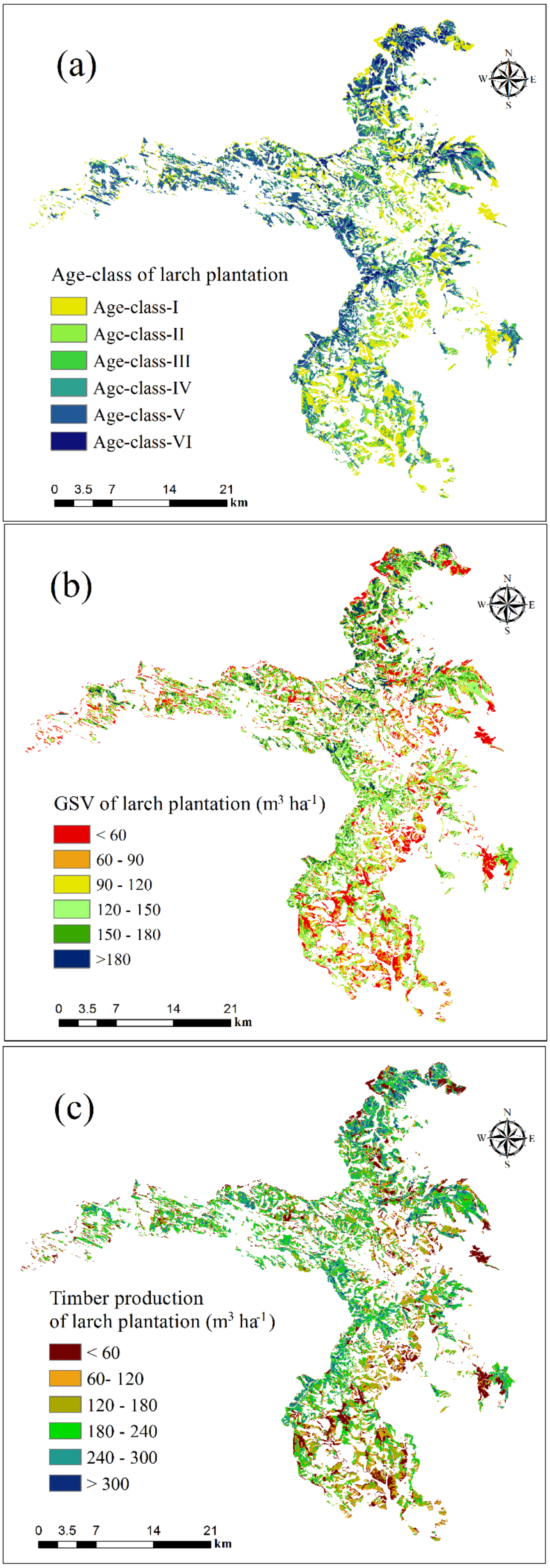
(a)
N
W
E
S
Age-class of larch plantation
Age-class-I
Age-class-II
Age-class-III
Age-class-IV
Age-class-V
Age-class-VI
0 3.5 7 14 21
km
(b)
N
W
E
S
GSV of larch plantation (m³ ha⁻¹)
< 60
60 - 90
90 - 120
120 - 150
150 - 180
>180
0 3.5 7 14 21
km
(c)
N
W
E
S
Timber production
of larch plantation (m³ ha⁻¹)
< 60
60- 120
120 - 180
180 - 240
240 - 300
> 300
0 3.5 7 14 21
km

Fig. 6 Spatial patterns of estimated age-classes (a) and GSV (b); Spatial patterns of timber production assessed by the management process–based timber production framework (c).

3.2 GSV of LP

The relationships of PALSAR backscatter with field-based GSV were established using statistical regression, and the HH- and HV-polarizations were used in training logarithmic models (γ^0 = a•log(GSV) + b). As shown in Fig. 7a, the fitted relationship for γ^0_{HV} was better than that for γ^0_{HH}, with R^2 of 0.75 and 0.66, respectively. The validation errors (RMSE) were estimated to be 36.5 m^3 ha^{-1} (relative RMSE is 28.7%) for γ^0_{HV} and 52.6 m^3 ha^{-1} (relative RMSE is 41.4%) for γ^0_{HH}, respectively (Fig. 7b).

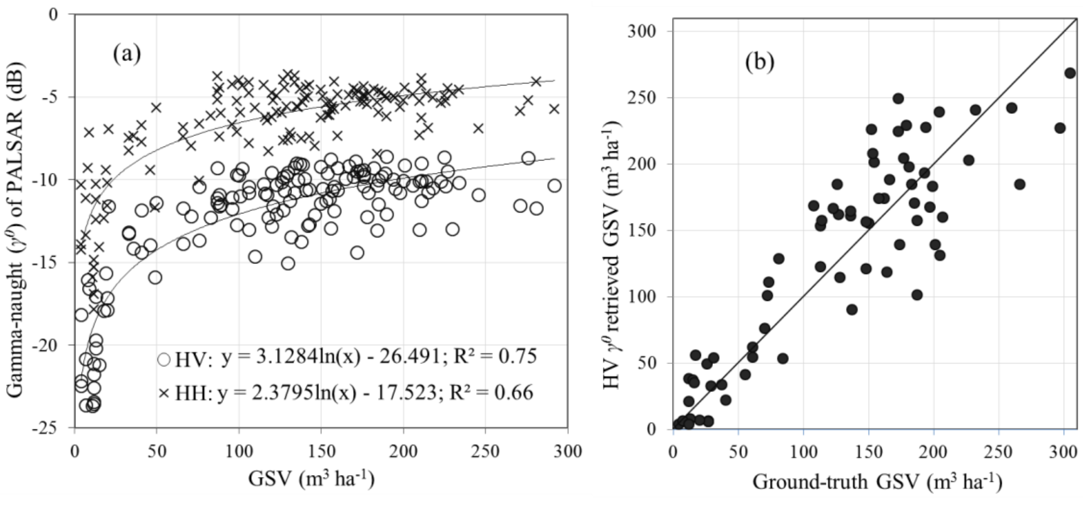

Fig. 7 Relationship between the PALSAR polarisations and GSV (a); Field-measured GSV against γ^0_{HV} retrieved GSV (b).

The promising regression model developed by γ^0_{HV} was used to map GSV of LP with a spatial resolution of 30 m (Fig. 6b). The total GSV of LP over a total area of 43,945 ha was estimated to be 4.87 × 10^6 m^3. The GSV density ranged approximately from less than 20 m^3 ha^{-1} to over 200 m^3 ha^{-1}, with an averaged value of 110.8 m^3 ha^{-1}. The analysis of six age-classes and corresponding GSVs suggested that the GSV increased with the age-classes, showing a robust positive correlation (R^2=0.61, P<0.05).

3.3 Timber production of LP

The timber production during a rotation period that combined current GSV and harvested timber derived from historical thinning operations was assessed for SFC. The total timber production of LP was estimated to be 7.27 × 10^6 m^3 for the period of 1962 to 2010, with 4.87 × 10^6 m^3 in current GSV and 2.40 × 10^6 m^3 in historical harvested timber, over a total area of 43,945 ha (Table 2). The historical process-harvested timber accounts to 33.0 % of the total timber production. The mean timber production density was 165.4 m^3 ha^{-1}, ranging from 20 to 350 m^3 ha^{-1}.

Table 2 Timber production of six sub-forestry centers. T1: sunny slope, 0~5°; T2: sunny slope, 5~10°; T3: sunny slope, 10~15°; T4: sunny slope, 15~20°; T5: shady 0~5°; T6: shady slope, 5~10°; T7: shady slope, 10~15°; T8: shady slope, 15~20°. I~VI refer to the six age-classes of LP.

Topographical types	Area (ha)	Density of harvested timber through thinning operation (m^3 ha^{-1})						Density of total timber production (m^3 ha^{-1})					
		I	II	III	IV	V	VI	I	II	III	IV	V	VI
T1	5985	0.0	17.2	45.7	68.5	97.0	123.3	44.5	159.6	160.0	210.6	228.9	269.3

T2	6850	0.0	17.8	45.3	69.3	97.9	125.7	49.7	155.5	165.0	212.2	236.9	271.3
T3	4407	0.0	19.5	46.2	69.0	97.3	125.2	56.2	152.6	160.6	210.1	237.2	270.7
T4	5499	0.0	19.2	45.4	65.8	93.1	119.0	58.0	150.5	147.4	202.0	222.9	265.5
T5	5633	0.0	16.0	42.7	65.5	93.6	120.2	44.5	149.3	156.6	206.1	226.6	265.4
T6	6341	0.0	18.1	44.9	68.7	97.3	126.0	51.5	152.2	163.7	211.5	241.0	277.0
T7	3994	0.0	20.7	47.3	71.4	100.2	129.7	66.3	153.8	167.5	215.4	247.9	284.7
T8	5236	0.0	24.3	51.0	74.8	103.4	132.6	83.5	157.7	170.0	217.6	249.6	291.6
Average	--	0.0	19.1	47.2	70.3	96.9	124.3	56.5	154.5	163.3	210.1	234.3	273.9

	Area (ha)	Averaged density of total timber production (m^3 ha^{-1})	Total timber production (10^4 m^3)
Total	43945	165.4	726.9

As descripted from Fig. 6c, a high-density timber production (>240 m^3 ha^{-1}) appeared in the north part of SFC. Additionally, the similar high-density (180 to 300 m^3 ha^{-1}) also observed in the middle part and western part of SFC. A medium timber production density (120 to 240 m^3 ha^{-1}) appeared throughout in SFC. The timber production in southeastern part has the lowest density (<120 m^3 ha^{-1}). Overall, the timber production of LP exhibits a large spatial heterogeneity and gradually decreases from northwest to southeast, showing an age-related spatial pattern.

4 Discussions

4.1 Feature selection for estimation of age-class

The feature selection based on the RF-based importance assessment of input variables reduced redundant variables (10 variables) and improved the classification accuracy (2.3%). The 10 removed variables included 7 variables for spring, 2 variables for summer and 1 variables for winter. It seems that variables of spring are not as useful as those in the other seasons. The capture date of image may be also important. Only 2 variables derived from Kauth–Thomas linear transformation was removed, indicating the transformed variables are more informative than the original bands (Fig. 8). The optimized subset included 16 spectral bands, 10 Kauth–Thomas linear transformation features and 2 PALSAR bands. The highest ranked variable in the optimized subset was near-infrared (NIR) band of summer. This result was consistent with the previous forest age classifications reported by Jensen et al. (1999) and Dye et al. (2012). The greenness and wetness of summer also showed strong predictive ability. The most important 3 variables appeared in summer, indicating the high importance of growing peak stage for discriminating age-classes of LP. It should be noted that, blue, red visible bands and greenness of autumn and blue visible band and brightness of winter were ranked in the most important 10 variables, which contributed more to the increase in accuracy than that of the same variables of summer. Our finding illustrated that the optical remotely sensed variables throughout a whole growing cycle were useful for capturing the reflectance differences among the

LP age-classes, due to mutual complementarity of multi-seasonal images. Furthermore, RF-based importance assessment ranked PALSAR HH and HV as the fourth and fifth important variables. Since PALSAR variables can characterize forest undercanopy structure, they were the critical supplement to optical variables for discrimination of LP age-classes. The combined subset of optical variables and PALSAR variables could be a powerful tool of improving classification accuracy of forest age.

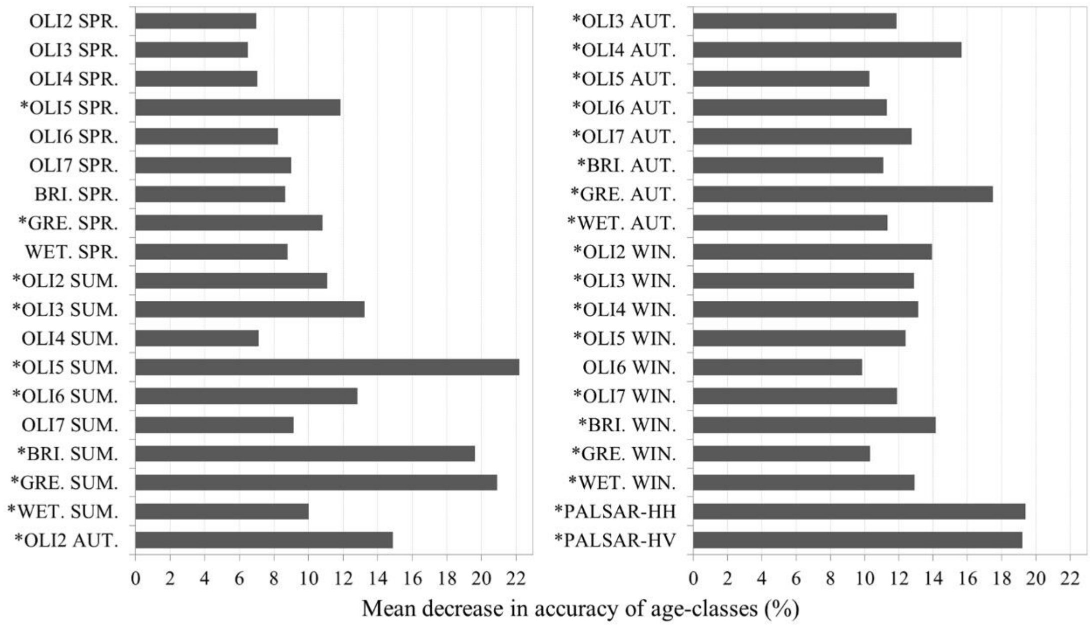

Fig. 8. Variable importance in optimized subset. BRI., GRE. and WET. refer to brightness, greenness and wetness, respectively. *: The 28 variables of the optimized subset.

4.2 Saturation effect for estimation of GSV

Although L-band backscatter intensity is strongly correlated with forest GSV, it is restricted by the saturation effect, which means the backscatter intensity loses its sensitivity to the increasing stand GSV when GSV exceed the saturation levels (Imhoff 1995). Saturation level is highly site dependent and has been reported to occur in a large GSV ranges mainly from 100 to 200 m^3 ha^{-1}, which concerned temperate and boreal forests (Peregon and Yamagata 2013; Chowdhury et al. 2014), mangrove (Hamdan et al. 2014), savanna (Mermoz et al. 2014), tropics (Saatchi et al. 2011), and plantation forests (Avtar et al. 2013). To our knowledge, however, there are no referenced studies that have been reported for LP. Generally, there are two quantitating definitions for saturation level: an increase in AGB of 1 Mg ha^{-1} corresponding to an increase of γ^{0}_{HV} smaller than 0.01 dB (Watanabe et al. 2006; Lucas et al. 2010), and an increase in AGB of 10 Mg.ha^{-1} corresponding to an increase of γ^{0}_{HV} smaller than 0.2 dB (Mermoz et al. 2014). To convert GSV (m^3 ha^{-1}) to AGB (Mg ha^{-1}), a special conversion function for larch was employed for marching the required unit (Wang et al. 2013); then the two definitions for saturation level were calculated. The result indicated that saturation levels for the two definitions were 327 m^3 ha^{-1} (310 Mg ha^{-1}) and 171 m^3 ha^{-1} (160 Mg ha^{-1}), respectively. In addition to these quantitating definitions, a simple comparison between truth GSV and retrieved GSV was also employed to define saturation level (Saatchi et al. 2011; Cartus et al. 2012; Chowdhury et al. 2014; Hamdan et al. 2014). Referring this method, the saturation level present in this study should be around 200 m^3 ha^{-1}. Note that, even though the lower saturation level (171 m^3 ha^{-1}) was considered, a small proportion (less than 12 %) of area was affected. If the saturation level of 200 m^3 ha^{-1} were taken into account, only 3% of area was affected. Therefore, it implied that the saturation effect on GSV estimation was rather limited.

Our observed saturation levels are higher than that observed in most previous studies. Soil, vegetation moist and forest structure are main factors that influence the saturation level (Lucas et al. 2010; Sandberg et al. 2011). On the one hand, the annul precipitation of SFC is approximately 450 mm, leading the low humidities of soil and vegetation. On the other hand, and perhaps more importantly, LP of SFC is single species monoculture, and the undergrowth (shrubs and small trees) is sparse, thereby producing a high proportion of tree stem-scattering (Watanabe et al. 2006). This simple structure can also mitigate the saturation effect in the GSV estimation.

4.3 Uncertainties of modelling timber production

The error of estimated GSV and age-class, which were the primary parameters of MPT framework, closely associated with uncertainties of modelling timber production. The RMSE for the GSV predictions was 36.5 m^3 ha^{-1}, which can be used to estimate the error in timber production directly. Furthermore, 32.1% of total pixels were supposed to be misclassified for age-class (Table 3), Since the age-classes were adopted for assessing the timber produced by thinning operation, the defined intervals of adjacent age-classes from Age-class-II to Age-class-V was small (5 years), which may cause difficulty on discrimination from one age-class to the adjacent another. This confusion between two age-classes leads to misestimated times of thinning operations. For example, if a pixel of Age-class-III LP is misclassified as Age-class-II, an underestimation would occur, because the timber that harvested by a thinning operation is not included in total timber production of the pixel. Similarly, if this pixel is misclassified as Age-class-V, the excessive harvested timber derived from two thinning operations is involved, leading to an overestimation of timber production.

Table 3 Errors in estimated timber production derived from the misclassification of age-classes. I~VI refer to the six age-classes of LP. Proportion of pixels refers to the misclassified proportion of total pixels for each age-class; Averaged times of thinning operations refers to averaged misestimated times of thinning operations for each age-class. For example, for the first record (overestimation for Age-class-I), a 1.3% of total pixels were misclassified as the higher age-classes; each of misclassified pixel was averagely overestimated for 3.3 times thinning operations, with an averaged harvested timber of 23.8 m^3 ha^{-1} for each thinning; the total overestimated timber was 4.9×10^4 m^3.

	Overestimation				
Age-class	Area (ha)	Proportion of pixels (%)	Averaged times of thinning operations	Averaged harvested timber for each thinning (m^3 ha^{-1})	Total harvested timber (10^4 m^3)
I	613.2	1.4	3.3	23.8	4.9
II	1635.2	3.7	3.0	26.0	12.8
III	2452.7	5.6	1.8	24.6	11.1
IV	1839.6	4.2	1.2	26.7	6.0
V	408.8	0.9	1.0	27.4	1.1

VI	0.0	0.0	0.0	0.0	0.0
Total	6949.4	15.8	-	-	35.8
	Underestimation				
Age-class	Area (ha)	Proportion of pixels (%)	Averaged times of thinning operations	Averaged harvested timber for each thinning (m^3 ha^{-1})	Total harvested timber (10^4 m^3)
I	0.0	0.0	0.0	0.0	0.0
II	408.8	0.9	1.0	19.1	0.8
III	1022.0	2.3	2.0	23.6	4.8
IV	1226.4	2.8	2.3	24.7	7.1
V	2248.3	5.1	2.0	24.8	11.2
VI	2248.3	5.1	1.2	27.3	7.2
Total	7153.8	16.3	-	-	31.1

As shown in Table 3, the proportion of overestimated age-class pixels was 15.8%, leading to an overestimated timber production of 35.8 × 10^4 m^3; the proportion of underestimated age-class pixels was 16.3%, leading to an underestimated timber production of 31.1 × 10^4 m^3. Comparing error in estimated GSV, the error derived from misclassification of age-class was small. Synthetically considering the RMSE (36.7 m^3 ha^{-1}) for estimated GSV and misclassification of age-class, the error in estimated timber production density ranged from -55.2 to 56.3 m^3 ha^{-1} (RMSE of estimated GSV was also considered for assessing error in historical harvested timber).

The difference between the MPT framework (Fig. 2) and practical thinning is another uncertainty source of timber production estimation. The MPT framework was localized for SFC, according to the general logging regime of LP. Nevertheless, the site conditions of LPs vary among topographies, leading to different LP productivities. Although the effect of site conditions on GSV was considered, various site conditions also associated with forest management. For example, LPs in very flat area probably experience more than five-time thinning operations with higher proportion of harvested timber, due to the high productivity as well as convenient practice condition. Conversely, LPs in mountain area may experience fewer thinning operations with less harvested timber. Considering the generally management measures for LP in SFC, this effect is only limited to part area of SFC.

5 Conclusion

This study demonstrates a Management Process–based Timber production framework that closely links to logging regimes of a plantation forest. The current GSV and harvested timber produced through historical thinning operations are combined to assess timber production of larch plantation during a rotation period (more than 40 years). The key parameters of the framework, including current GSV and age-class, were estimated by field-based samples and multi-source remote sensing data, and total timber production of larch plantation has been assessed with the MPT framework. This approach can assess timber production during a long term without historical data. It is noteworthy that the framework was specially designed for the management regime of larch plantation in Saihanba Forestry Center. It can also be widely used for assessing timber production in other area, with localized proxies according the forest management regimes. This approach can provide crucial information for a better understanding of forest ecosystem service functions.

The saturation effect of the PALSAR signal for GSV is observed at a high level, both due to dry environment of the vegetation and simple structure of larch plantation. Considering the large area of plantation forests and its increasing trend in China, ALOS PALSAR has the potential to be an excellent dataset for plantation forest monitoring. The analysis of uncertainties has shown that the error in estimated GSV contributes a larger proportion of error in timber production than that of age-class. Another possible uncertainty is from the difference between the management practices and the MPT framework, although its effect would be small. Future study should elaborate diverse designs linking to various forest management measures for different tree species.

Acknowledgements

This research was supported by the National Basic Research Program of China (973 Program, No. 2012CB416906) and National Natural Science Foundation of China (No. 31500466). We would like to acknowledge Shun Cheng of the Saihanba Forestry Center for providing the Forest Resource Management Inventory data, and we are grateful to Dr. Xinhua Zhou's constructive suggestions on the revised manuscript.

References

Adam, E., Mutanga, O., Abdel-Rahman, E.M., & Ismail, R., 2014. Estimating standing biomass in papyrus (*Cyperus papyrus L.*) swamp: exploratory of in situ hyperspectral indices and random forest regression. Int. J. Remote Sens. 35(2), 693-714.

Alkemade, R., Burkhard, B., Crossman, N.D., Nedkov, S., & Petz, K., 2014. Quantifying ecosystem services and indicators for science, policy and practice. Ecological Indicators 37, Part A, 161-162.

Almeida Filho, R., Rosenqvist, A., Shimabukuro, Y.E., & Silva Gomez, R., 2007. Detecting deforestation with multitemporal L-band SAR imagery: a case study in western Brazilian Amazonia. Int. J. Remote Sens. 28(6), 1383-1390.

Anaya, J.S.A., Chuvieco, E., & Palacios-Orueta, A., 2009. Aboveground biomass assessment in Colombia: A remote sensing approach. Forest Ecol. Manag. 257(4), 1237-1246.

Avtar, R., Takeuchi, W., & Sawada, H., 2013. Monitoring of biophysical parameters of cashew plants in Cambodia using ALOS/PALSAR data. Environ. Monit. Assess. 185(2), 2023-2037.

Bijalwan, A., Swamy, S.L., Sharma, C., Sharma, N., & Tiwari, A.K., 2010. Land-use, biomass and carbon estimation in dry tropical forest of Chhattisgarh region in India using satellite remote sensing and GIS. Journal of Forestry Research 21(2), 161-170.

Breiman, L., 2001. Random Forests. Mach. Learn. 45(1), 5-32.

Carreiras, J.O.M.B., Vasconcelos, M.J., & Lucas, R.M., 2012. Understanding the relationship between aboveground biomass and ALOS PALSAR data in the forests of Guinea-Bissau (West Africa). Remote Sens. Environ. 121, 426-442.

Cartus, O., Santoro, M., & Kellndorfer, J., 2012. Mapping forest aboveground biomass in the Northeastern United States with ALOS PALSAR dual-polarization L-band. Remote Sens. Environ. 124, 466-478.

Chowdhury, T.A., Thiel, C., & Schmullius, C., 2014. Growing stock volume estimation from L-band ALOS PALSAR polarimetric coherence in Siberian forest. Remote Sens. Environ. 155, 129-144.

Costanza, R., D'Arge, R., de Groot, R., Farber, S., Grasso, M., Hannon, B., Limburg, K., Naeem, S., O'Neill, R.V., Paruelo, J., Raskin, R.G., Sutton, P., & van den Belt, M., 1997. The value of the world's ecosystem services and natural capital. Nature 387(6630), 253-260.

Davis, S.C., Hessl, A.E., Scott, C.J., Adams, M.B., & Thomas, R.B., 2009. Forest carbon sequestration changes in response to timber harvest. Forest Ecol. Manag. 258(9), 2101-2109.

Diaz-Uriarte, R., & Alvarez De Andres, S., 2006. Gene selection and classification of microarray data using random forest. BMC Bioinformatics 7(1), 3.

Dye, M., Mutanga, O., & Ismail, R., 2012. Combining spectral and textural remote sensing variables using random forests: predicting the age of Pinus patula forests in KwaZulu-Natal, South Africa. Journal of Spatial Science 57(2), 193-211.

Fang, J., Chen, A., Peng, C., Zhao, S., & Ci, L., 2001. Changes in forest biomass carbon storage in China between 1949 and 1998. Science 292(5525), 2320-2322.

Fang, J, Liu, G, & Xu, S, 1996. Biomass and net production of forest vegetation in China. Acta Ecologica Sinica 16(5), 497-508. (In Chinese)

Chinese Ministry of Forestry, 2014. Forest resource statistics of China. Beijing, China: Department of Forest Resource and Management. (In Chinese)

Forshed, O., Karlsson, A., Falck, J., & Cedergren, J., 2008. Stand development after two modes of selective logging and pre-felling climber cutting in a dipterocarp rainforest in Sabah, Malaysia. Forest Ecol. Manag. 255(3-4), 993-1001.

Fu, B., & Forsius, M., 2015. Ecosystem services modeling in contrasting landscapes. Landscape Ecol. 30(3), 375-379.

Galeana-Pizaña, J.M., López-Caloca, A., López-Quiroz, P., Silván-Cárdenas, J.L., & Couturier, S., 2014. Modeling the spatial distribution of above-ground carbon in Mexican coniferous forests using remote sensing and a geostatistical approach. Int. J. Appl. Earth Observ. Geoinform. 30, 179-189.

Gao, T., Yang, X., Jin, Y., Ma, H., Li, J., Yu, H., Yu, Q., Zheng, X., & Xu, B., 2013a. Spatio-temporal variation in vegetation biomass and its relationships with climate factors in the Xilingol grasslands, Northern China. PLoS ONE 8(12), e83824.

Gao, T., Zhu, J., Zheng, X., Shang, G., Huang, L., & Wu, S., 2015. Mapping spatial distribution of larch plantations from multi-seasonal Landsat-8 OLI imagery and multi-scale textures using Random Forests. Remote Sensing 7(2), 1702-1720.

Gao, Y., Liu, X., Min, C., He, H., Yu, G., Liu, M., Zhu, X., & Wang, Q., 2013b. Estimation of the North-South Transect of Eastern China forest biomass using remote sensing and forest inventory data. Int. J. Remote Sens. 34(15), 5598-5610.

Grimm, R., Behrens, T., M rker, M., & Elsenbeer, H., 2008. Soil organic carbon concentrations and stocks on Barro Colorado Island—digital soil mapping using Random Forests analysis. Geoderma 146(1-2), 102-113.

Hamdan, O., Khali Aziz, H., & Mohd Hasmadi, I., 2014. L-band ALOS PALSAR for biomass estimation of Matang Mangroves, Malaysia. Remote Sens. Environ. 155, 69-78.

He, Q., Cao, C., Chen, E., Sun, G., Ling, F., Pang, Y., Zhang, H., Ni, W., Xu, M., Li, Z., & Li, X., 2011. Forest stand biomass estimation using ALOS PALSAR data based on LiDAR-derived prior knowledge in the Qilian Mountain, western China. Int. J. Remote Sens. 33(3), 710-729.

Houghton, R.A., Butman, D., Bunn, A.G., Krankina, O.N., Schlesinger, P., & Stone, T.A., 2007. Mapping Russian forest biomass with data from satellites and forest inventories. Environmental Research Letters 2(4), 45032.

Imhoff, M.L., 1995. Radar backscatter and biomass saturation: ramifications for global biomass inventory. Geoscience and Remote Sensing, IEEE Transactions on 33(2), 511-518.

Ismail, R., Mutanga, O., & Kumar, L., 2010. Modeling the potential distribution of pine forests susceptible to *Sirex Noctilio* infestations in Mpumalanga, South Africa. Transactions in GIS 14(5), 709-726.

Ismail, R., & Mutanga, O., 2010. A comparison of regression tree ensembles: Predicting *Sirex noctilio* induced water stress in *Pinus patula* forests of KwaZulu-Natal, South Africa. Int. J. Appl. Earth Observ. Geoinform. 12, Supplement 1, S45-S51.

Jenkins, J.C., Chojnacky, D.C., Heath, L.S., & Birdsey, R.A., 2003. National-scale biomass estimators for United States tree species. For. Sci. 49:12-39.

Jensen, J.R., Qiu, F., & Ji, M. Predictive modelling of coniferous forest age using statistical and artificial neural network approaches applied to remote sensor data. In (pp. 2805-2822)

Karam, M.A., Amar, F., Fung, A.K., Mougin, E., Lopes, A., Le Vine, D.M., & Beaudoin, A., 1995. A microwave polarimetric scattering model for forest canopies based on vector radiative transfer theory. Remote Sens. Environ. 53(1), 16-30.

Lawrence, R.L., Wood, S.D., & Sheley, R.L., 2006. Mapping invasive plants using hyperspectral imagery and Breiman Cutler classifications (Random Forest). Remote Sens. Environ. 100(3), 356-362.

Lee, J.S., Wen, J.H., Ainsworth, T., Chen, K.S., & Chen, A., 2009. Improved sigma filter for speckle filtering of SAR imagery. IEEE T. Geosci. Remote 47, 202-213.

Li, D., Ju, W., Fan, W., & Gu, Z., 2014b. Estimating the age of deciduous forests in northeast China with Enhanced Thematic Mapper Plus data acquired in different phenological seasons. Journal of Applied Remote Sensing 8(1), 83670.

Li, Y., Ye, S., Hui, G., Hu, Y., & Zhao, Z., 2014a. Spatial structure of timber harvested according to structure-based forest management. Forest Ecol. Manag. 322, 106-116.

Liaw, A., & Wiener, M., 2002. Classification and regression by random forest. R News 2/3, 18-22.

Liesenberg, V., & Gloaguen, R., 2013. Evaluating SAR polarization modes at L-band for forest classification purposes in Eastern Amazon, Brazil. Int. J. Appl. Earth Observ. Geoinform. 21, 122-135.

Lucas, R.M., Armston, J., Fairfax, R., Fensham, R., Accad, A., Carreiras, J., & Authors, M., 2010. An evaluation of the ALOS PALSAR L-band backscatter-above ground biomass relationship Queensland, Australia: impacts of surface moisture condition and vegetation structure. IEEE Journal of Selected Topics in Applied Earth Observations and Remote Sensing 4(3), 576-593.

Luo, X., He, H., Liang, Y., Wang, W., Wu, Z., & Fraser, J., 2014. Spatial simulation of the effect of fire and harvest on aboveground tree biomass in boreal forests of Northeast China. Landscape Ecol. 29(7), 1187-1200.

Mason, W.L., & Zhu, J.J. (Eds.), 2014. Silviculture of planted forests managed for multi-functional objectives: lessons from Chinese and British experiences. Dordrecht: Springer science business media Dordrecht.

Mermoz, S.P., Le Toan, T., Villard, L., R jou-M chain, M., & Seifert-Granzin, J., 2014. Biomass assessment in the Cameroon savanna using ALOS PALSAR data. Remote Sens. Environ. 155, 109-119.

Morel, A.C., Saatchi, S.S., Malhi, Y., Berry, N.J., Banin, L., Burslem, D., Nilus, R., & Ong, R.C., 2011.

Estimating aboveground biomass in forest and oil palm plantation in Sabah, Malaysian Borneo using ALOS PALSAR data. Forest Ecol. Manag. 262(9), 1786-1798.

Naidoo, L., Cho, M.A., Mathieu, R., & Asner, G., 2012. Classification of savanna tree species, in the Greater Kruger National Park region, by integrating hyperspectral and LiDAR data in a Random Forest data mining environment. ISPRS J. Photogramm. 69, 167-179.

Nunery, J.S., & Keeton, W.S., 2010. Forest carbon storage in the northeastern United States: Net effects of harvesting frequency, post-harvest retention, and wood products. Forest Ecol. Manag. 259(8), 1363-1375.

Pan, Y., Birdsey, R.A., Fang, J., Houghton, R., Kauppi, P.E., Kurz, W.A., Phillips, O.L., Shvidenko, A., Lewis, S.L., Canadell, J.G., Ciais, P., Jackson, R.B., Pacala, S., McGuire, A.D., Piao, S., Rautiainen, A., Sitch, S., & Hayes, D., 2011. A large and persistent carbon sink in the world's forests. Science 333, 988-993.

Peregon, A., & Yamagata, Y., 2013. The use of ALOS/PALSAR backscatter to estimate above-ground forest biomass: A case study in Western Siberia. Remote Sens. Environ. 137, 139-146.

Ray, D.G., Seymour, R.S., Scott, N.A., & Keeton, W.S., 2009. Mitigating climate change with managed forests: balancing expectations, opportunity, and risk. J. Forest. 107, 50-51.

Rodriguez-Galiano, V., & Chica-Olmo, M., 2012. Land cover change analysis of a Mediterranean area in Spain using different sources of data: Multi-seasonal Landsat images, land surface temperature, digital terrain models and texture. Applied Geography 35(1-2), 208-218.

Rodriguez-Galiano, V.F., Chica-Olmo, M., Abarca-Hernandez, F., Atkinson, P.M., & Jeganathan, C., 2012. Random Forest classification of Mediterranean land cover using multi-seasonal imagery and multi-seasonal texture. Remote Sens. Environ. 121, 93-107.

Rosenqvist, A., Shimada, M., Ito, N., & Watanabe, M., 2007. ALOS PALSAR: A pathfinder mission for global-scale monitoring of the environment. Geoscience and Remote Sensing, IEEE Transactions on 45(11), 3307-3316.

Roy, D.P., Wulder, M.A., Loveland, T.R., C. E., W., Allen, R.G., Anderson, M.C., Helder, D., Irons, J.R., Johnson, D.M., Kennedy, R., Scambos, T.A., Schaaf, C.B., Schott, J.R., Sheng, Y., Vermote, E.F., Belward, A.S., Bindschadler, R., Cohen, W.B., Gao, F., Hipple, J.D., Hostert, P., Huntington, J., Justice, C.O., Kilic, A., Kovalskyy, V., Lee, Z.P., Lymburner, L., Masek, J.G., McCorkel, J., Shuai, Y., Trezza, R., Vogelmann, J., Wynne, R.H., & Zhu, Z., 2014. Landsat-8: Science and product vision for terrestrial global change research. Remote Sens. Environ. 145, 154-172.

Saatchi, S., Marlier, M., Chazdon, R.L., Clark, D.B., & Russell, A.E., 2011. Impact of spatial variability of tropical forest structure on radar estimation of aboveground biomass. Remote Sens. Environ. 115(11), 2836-2849.

Saihanba Forestry Center, 2012. Forest resource plan and inventory report (4th) of Saihanba Forestry Center of Hebei province. Hebei, China: Saihanba Forestry Center. (In Chinese)

Sandberg, G., Ulander, L.M.H., Fransson, J.E.S., Holmgren, J., & Le Toan, T., 2011. L- and P-band backscatter intensity for biomass retrieval in hemiboreal forest. Remote Sens. Environ. 115(11), 2874-2886.

Santoro, M., Beer, C., Cartus, O., Schmullius, C., Shvidenko, A., McCallum, I., Wegm ller, U., & Wiesmann, A., 2011. Retrieval of growing stock volume in boreal forest using hyper-temporal series of Envisat ASAR ScanSAR backscatter measurements. Remote Sens. Environ. 115(2), 490-507.

Santoro, M., Eriksson, L., & Fransson, J., 2015. Reviewing ALOS PALSAR Backscatter observations for stem volume retrieval in Swedish Forest. Remote Sensing 7(4), 4290-4317.

Shimada, M., Isoguchi, O., Tadono, T., & Isono, K., 2009. PALSAR radiometric and geometric calibration. IEEE Transaction on Geosciences and Remote Sensing 47(2), 3915-3932.

Shimada, M., Itoh, T., Motooka, T., Watanabe, M., Shiraishi, T., Thapa, R., & Lucas, R., 2014. New global forest/non-forest maps from ALOS PALSAR data (2007-2010). Remote Sens. Environ. 15, 13-31.

Shimada, M., & Ohtaki, T., 2010. Generating large-scale high-quality SAR mosaic datasets: Application to PALSAR data for global monitoring. IEEE Journal of Selected Topics in Applied Earth Observations and Remote Sensing 3(4), 637-656.

Simard, M., Grandi, G.D., Saatchi, S., & Mayaux, P., 2002. Mapping tropical coastal vegetation using JERS-1 and ERS-1 radar data with a decision tree classifier. Int. J. Remote Sens. 23(7), 1461-1474.

Suzuki, R., Kim, Y., & Ishii, R. Sensitivity of the backscatter intensity of ALOS/PALSAR to the above-ground biomass and other biophysical parameters of boreal forest in Alaska. In (pp. 100-112)

Tinkham, W.T., Smith, A.M.S., Marshall, H., Link, T.E., Falkowski, M.J., & Winstral, A.H., 2014. Quantifying spatial distribution of snow depth errors from LiDAR using Random Forest. Remote Sens. Environ. 141, 105-115.

Wang, X., Ouyang, S., Sun, O.J., & Fang, J., 2013. Forest biomass patterns across northeast China are strongly shaped by forest height. Forest Ecol. Manag. 293, 149-160.

Watanabe, M., Shimada, M., Rosenqvist, A., Tadono, T., Matsuoka, M., Romshoo, S.A., Ohta, K., Furuta, R., Nakamura, K., & Moriyama, T., 2006. Forest structure dependency of the relation between l-band sigma and biophysical parameters. Geoscience and Remote Sensing, IEEE Transactions on 44(11), 3154-3165.

Way, J., Rignot, E.J.M., McDonald, K.C., Oren, R., Kwok, R., Bonan, G., Dobson, M.C., Viereck, L.A., & Roth, J.E., 1994. Evaluating the type and state of Alaska taiga forests with imaging radar for use in ecosystem models. Geoscience and Remote Sensing, IEEE Transactions on, 32(2), 353-370.

Yan, Q., Zhu, J.J., & Gang, Q., 2013. Comparison of spatial patterns of soil seed banks between larch plantations and adjacent secondary forests in Northeast China: implication for spatial distribution of larch plantations. Trees 27(6), 1747-1754.

Yimer, F., Ledin, S., & Abdelkadir, A., 2006. Soil property variations in relation to topographic aspect and vegetation community in the south-eastern highlands of Ethiopia. Forest Ecol. Manag. 232(1-3), 90-99.

Zeng, W., & Zhou, Y., 2003. Discussion on main problems and countermeasures to continuous forest inventory and forest management inventory. Central South Forest Inventory and Planning 22(22), 21-29. (In Chinese)

Zheng, S., Cao, C., Dang, Y., Xiang, H., Zhao, J., Zhang, Y., Wang, X., & Guo, H., 2013. Retrieval of forest growing stock volume by two different methods using Landsat TM images. Int. J. Remote Sens. 35(1), 29-43.

Zhu, J.J., Yang, K., Yan, Q., Liu, Z., Yu, L., & Wang, H., 2010. Feasibility of implementing thinning in even-aged *Larix olgensis* plantations to develop uneven-aged larch-broadleaved mixed forests. Journal of Forest Research 15(1), 71-80.

Zou, Y., Sang, W., Wang, S., Warren-Thomas, E., Liu, Y., Yu, Z., Wang, C., & Axmacher, J.C., 2015. Diversity patterns of ground beetles and understory vegetation in mature, secondary, and plantation forest regions of temperate northern China. Ecology and Evolution 5(3), 531-542.